A Numerical Model for Wall Heat Transfer Associated with Exothermic Reaction in SI Engine Combustion Chambers

K.Nishiwaki and T.Kojima

Department of Mechanical Engineering
Ritsumeikan University
1916 Nojicho, Kusatsu, Shiga 525-77
Japan

ABSTRACT

A numerical heat transfer model has been formulated that treats with exothermic reaction and quenching in thermal boundary layers in s. i. engine combustion chambers. The combustion model is made up of a two-stage process with a three-zone concept for a temperature field within each computational cell, describing not only the combined turbulence/reaction-controlled combustion in a near wall region but the turbulence-controlled combustion in a core region. The numerical technique features an additional grid system in the cells adjacent to the walls giving boundary layer resolution. The present model has reproduced the experimental evidence presented in literatures that the local heat flux peaks higher in insulated s. i. engines than in conventional s. i. engines, while the law of the wall has not predict the fact.

INTRODUCTION

The knowledge of thermal behaviors in reacting thermal boundary layers is essential in terms of the analysis of wall heat transfer, quench, pollutant formation and knock in s. i. engines. The combustion process in the near wall regions takes place under the combined turbulence/reaction-control, followed by quench in very close vicinity to the wall. Satisfactory numerical studies have not been made for analyzing heat transfer in such a situation.

The law of the wall has been widely used as a standard model for the wall boundary condition in the CFD codes, though it is valid for the steady turbulent boundary layers without exothermic reaction. There have been two models presented to deal with unsteady reacting thermal boundary layers in i. c. engines. One is the model of an approximate one-dimensional analytical solution presented by Yang and Martin[1] and the other is a numerical model with an additional boundary layer grid system presented by Jennings[2]. The former may not be said a real simulation of the reacting thermal boundary layer, because the quench distance was assumed. The latter did not reproduce the experimental evidence indicated in the literatures[3,4] that the local heat flux peaks higher as the wall temperature increases in s. i. engines.

The present study aims at developing a heat transfer model which solves thermal behaviors in reacting thermal boundary layers in a premixed combustion process.

BRIEF DESCRIPTION OF GOVERNING EQUATIONS

The governing equations are those described with cylindrical co-ordinates in an axisymmetric field for general conservation of mass, momentum, enthalpy, turbulent kinetic energy, its dissipation rate and the mass fractions of fuel, reactants and products. The mass fraction of the reactants is a special variable in the present combustion model which will be explained later.

The standard k-ε two-equation model is used for describing turbulence with the empirical coefficients presented by Morel-Mansour[5] including the dilatation effect.

COMBUSTION MODEL

The requirement for the combustion model in the present study is to describe turbulence/reaction-controlled combustion in the near wall region as well as the turbulence-controlled combustion in the core region. To take this into account, the model is constructed of a two-stage process or a turbulent mixing followed by an exothermic reaction. The stoichiometric mixture combustion is analyzed for simplicity in the present study.

At the first stage, an unburned fuel-air mixture is entrained in the fine structures which exist at the interface between unburned and burned gases in a turbulence energy dissipation process. The entrained portion of the fuel-oxygen mixture is called the "reactants" in the present text. The mass production rate of the reactants, R_m, is modeled in the manner similar to the eddy dissipation concept of Magnussen[6,7] as follows:

$$R_m = (1+S)\, r_{en}\, \frac{\chi}{1-\chi\gamma^*}\, \frac{\rho m_{fu}}{\gamma_\lambda} \qquad [kg/(m^3 \cdot s)] \quad (1)$$

$$\frac{m_{fu}}{\gamma_\lambda} \le m_{fu,st}\ ;\ \chi \le 1\ ;\ \gamma^* < 1$$

where,

- r_{en} : mass production rate of fine structures per unit mass of gas, [1/s]
- m_{fu} : mass fraction of fuel
- $m_{fu,st}$: stoichiometric fuel mass fraction
- S : stoichiometric oxygen requirement of fuel
- ρ : cell average density, [kg/m^3]

γ^* : mass fraction occupied by fine structures
γ_λ : mass fraction occupied by fine structure regions
χ : mass fraction of fine structures producing reactants

At the second stage, the reactants are consumed at the rate, R_c, described by the one step reaction as shown below:

$$R_c=(1+S)\frac{m_{re}}{m_{re}^*}\frac{T_r}{T_{av}}R_c^* \qquad [kg/(m^3\cdot s)] \quad (2)$$

$$R_c^*=M_{fu}\,F\,X_{fu}^{\ a}\,X_{ox}^{\ b}\exp(-D/T_r) \quad [kg/(m^3\cdot s)] \quad (2a)$$

where,
R_c^* : fuel mass consumption rate per unit volume of reactants
D : activation temperature
F : collision factor
M_{fu} : molecular weight of fuel
m_{re} : mass fraction of reactants
m_{re}^* : mass fraction of fuel and oxygen in fuel-air mixture
X : mole concentration in reactants
T_{av} : cell average temperature
T_r : effective reaction temperature,
and subscripts *fu* and *ox* refer to fuel and oxygen, respectively. The constants in Eq.(2a) were taken from the empirical reaction rate for octane presented by Westbrook[8] as given below:

$F=4.6\times10^{11}\,[(\mathrm{mol/cm^3})^{(1-a-b)}\cdot\mathrm{s^{-1}}]$, $D=15100$ [K]
$a=0.25$, $b=1.5$

The source terms in the general conservation equations for the mass fractions of fuel, reactants and products are given by the use of Eqs. (1) and (2) as shown below with the symbols S_{fu}, S_{re} and S_{pr}, respectively.

$$S_{fu}=-R_m/(1+S)\ ;\ S_{re}=R_m-R_c\ ;\ S_{pr}=R_c \qquad (3)$$

The effective reaction temperature, T_r, in Eq. (2a) is not always the cell average temperature, T_{av}, which is given by the energy equation. Figure 1 illustrates a three-zone

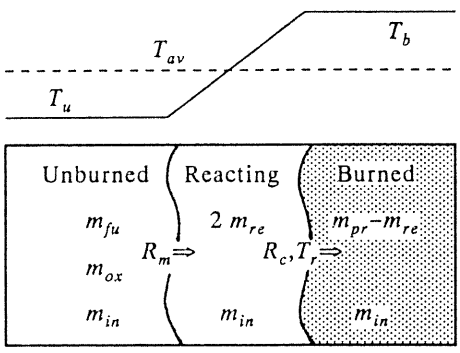

Fig. 1 Three-zone model for a sub-grid temperature field

model for a temperature field in each computational cell. The subscripts *pr* and *in* refer to products and inerts, respectively. The temperature field is modeled to be made up of an unburned fuel-air mixture temperature, T_u, a products temperature, T_b, and a reacting region temperature, T_r, which lies between T_u and T_b. Since the reaction rate has an exponential dependence on temperature, it can be assumed for simplicity that the effective reaction temperature T_r is equal to T_b.

In the core region, where the fast chemistry is applied, T_r or T_b can be assumed a local adiabatic flame temperature. In the near wall region, however, the reaction becomes slower due to the lower temperature in boundary layers, while the production of the fine structures is accelerated by the viscous effect which makes the turbulent kinetic energy dissipate faster. When the reaction needs a longer time than the residence time of the fine structures, the reactants leave the state of the fine structures before they reach a local adiabatic flame temperature and continue to react in the surroundings. The reactants in the surroundings may complete reaction there or have a chance to make another fine structures with the unburned mixture. Thus the intermediate reactants will appear that are composed of the unburned mixture mixed with still reacting "products". In this manner the cell composition comes towards a homogeneous state, T_r or T_b being lower than a local adiabatic flame temperature and closer to the cell average temperature.

To take these considerations into account, the weighting function w, which varies from zero to unity, is introduced. With the assumption that the reacting region is composed of the reactants and the same mass of the products as indicated in Fig. 1, the temperature T_r or T_b can be written as follows:

$$T_r=\frac{1}{c_p}\left(h_{av}+\frac{m_{fu}+m_{ox}+m_{re}}{1-m_{in}}\,w\frac{H_u}{1+L}\right) \qquad (4)$$

where,
c_p : specific heat at constant pressure
h_{av} : cell average enthalpy
H_u : lower heating value
L : theoretical air

A similar model can be applied to the mole concentration of species, X, in Eq. (2a) as given below:

$$X_{fu}=\frac{1}{1+S}\{m_{re}+w(m_{re}^*-m_{re})\}\frac{\rho}{M_{fu}} \qquad (5)$$

$$X_{ox}=\frac{S}{1+S}\{m_{re}+w(m_{re}^*-m_{re})\}\frac{\rho}{M_{ox}} \qquad (6)$$

The weighting function w is formulated so as to reflect

the reaction rate and the production rate of the fine structure as described in the following. The production rate of the fine structures per unit mass of the fine structures, r_{fs}, is given by[7],

$$r_{fs}=2.43(\varepsilon/\nu)^{1/2} \qquad [1/s] \tag{7}$$

where ν denotes kinematic viscosity.

Then the production rate of fuel entrained in the fine structures per unit volume of the reactants, R_m^*, can be written as follows;

$$R_m^* = r_{fs}\,\frac{1}{1-\chi\gamma^*}\rho\,\frac{T_{av}}{T_r}\,\frac{1}{1+L} \qquad [kg/(m^3\cdot s)] \tag{8}$$

Using Eqs. (2a) and (8), the weighting function w is assumed to have the form as;

$$w=\frac{R_c^*}{R_m^*} \quad ; \quad w\le 1 \tag{9}$$

The above equation is applied only to the grid cells adjacent to the wall where additional fine grid systems are placed as mentioned later. In conventional grid cells w is assumed unity, because the transition of w from 1 to 0 or vice versa takes place in so small a distance that the conventional grid cells can not afford such a resolution.

MODEL FOR THE TURBULENCE CHARACTERISTICS IN THE NEAR WALL REGION

The turbulent characteristics in the near wall region are known to be different from those in the core region because of the augmented dissipation rate of turbulence exerted by molecular viscosity. Applying a low Reynolds number model of the $k-\varepsilon$ equations may be one of the methods to take this into account. However, an empirical model was adopted in the near wall region for simplicity and for stable computation of turbulence variables in very close vicinity to the wall. An empirical equation for the turbulent viscosity ν_t is given by[9],

$$\nu_t/\nu = Ky^+\{1-\exp(-2aKy^+)\} \tag{10}$$
$$a=0.06, \quad y^+=\rho u_f/\mu$$

where u_f is the friction velocity.

With the assumption that the turbulence integral scale is proportional to the distance from the wall surface, y, the dissipation rate of the turbulent kinetic energy, ε, is written in the form as,

$$\varepsilon = c_\mu^{3/4}k^{3/2}/(Ky) \quad ; \quad K=0.4,\ c_\mu=0.09 \tag{11}$$

The turbulence variables k and ε in the near wall region can be obtained by combining Eqs. (10), (11) and the relation $\nu_t/\nu = c_\mu k^2/\varepsilon$.

COMPUTATIONAL GRID SYSTEM

Figure 2 shows the computational grid system which is composed of the conventional grids and the near wall grids added to each grid cell adjacent to the wall. The number of conventional grid cells used in the present calculations was 40 in the radial direction and varied from 20 to 80 in the axial direction with crank angle. The size of the near wall grid spacing is progressively halved in the normal direction to the wall as it approaches to the wall surface. Each cell adjacent to the wall included 10 or 11 near wall cells in the grid free condition. The minimum size of the near wall grid spacing was an order of micron. This technique allows to perform the computations in a practical length of time with boundary layer resolution.

NUMERICAL PROCEDURE

The numerical solution method employed the semi-implicit scheme for the continuity and the momentum equations for all grid cells including the grid cells adjacent to the wall which are treated as the conventional cells not having the near wall grid cells. The method allows a usual pressure correction procedure without any special consideration for the near wall grid cells. Other scaler variables are solved explicitly except those in the near wall grid cells.

The solution method for the variables in the near wall grid cells is as follows. The velocity component parallel to the wall are given by the law of the wall which takes the cell average value as the basis. The velocity component normal to the wall is solved from the continuity equation with the assumption of uniform pressure field in each cell. Other scaler variables are solved by the fully implicit scheme for the normal direction and by the explicit scheme for the parallel direction.

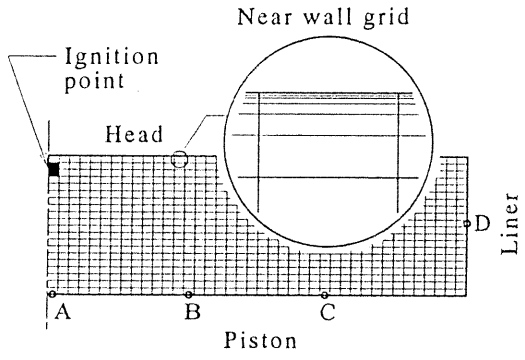

Fig. 2 Computational grid system showing conventional grids and near wall grids

COMPUTED RESULTS AND DISCUSSIONS

Comparison with Motored Engine Data

The data used for comparison was taken from the study presented by Dao et al.[10] The measurement was performed on an engine having a pancake combustion chamber geometry with a bore of 79.4 mm, a stroke of 101.6 mm and a compression ratio of 14. The engine was motored at 900 rpm with the initial swirl ratio of 7.2. Figure 3 shows the measured local heat fluxes at two different locations on the cylinder head surface and the computed results; r denotes the radial distance from the cylinder axis. Good agreement is seen between the measured and computed results. The figure also shows the computed results obtained by using the law of the wall instead of the near wall grid method. It is indicated that the two models give nearly the same result.

Wall Temperature Dependence of Heat Transfer during Combustion Process

The engine dimensions used for the computation are a bore of 83 mm, a stroke of 83.6 mm and a compression ratio of 8.8 with a pancake combustion chamber. The compression began at −135 °CA with the initial swirl ratio of 2 and an engine speed of 3000 rpm. The ignition was given at −17 °CA. The wall temperatures were set to be uniform and constant. The computations were performed with three different wall temperatures of 523 K, 873 K and 1073 K. The former wall temperature was taken as a typical value seen in conventional engines and the latter two were selected to be typically seen in insulated engines.

Figure 4 shows temperature fields at several selected crank angles of interest, computed for the conventional wall temperature. The flame propagation is seen to begin at −15 °CA, just after the ignition, then grow at −10 °CA and

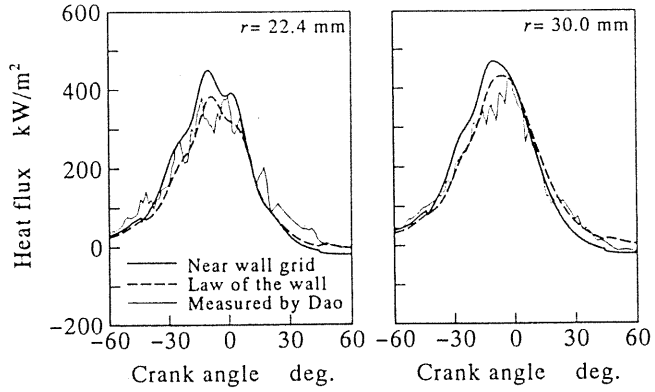

Fig. 3 Comparison of computed local heat fluxes with experimental results by Dao et al.[10] for a motored engine

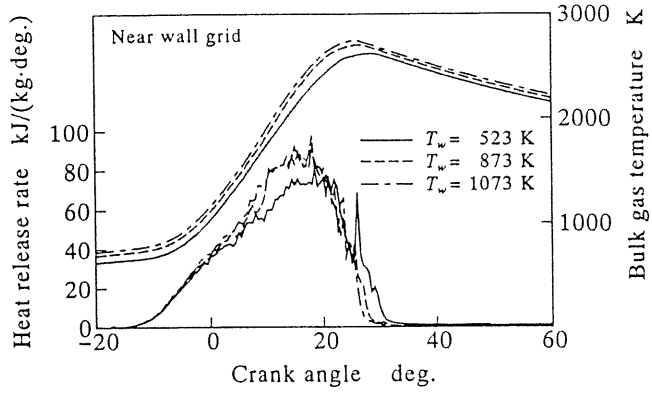

Fig. 5 Heat release rates and bulk gas temperatures computed by the present model (near wall grid method) and the law of the wall for different wall temperatures

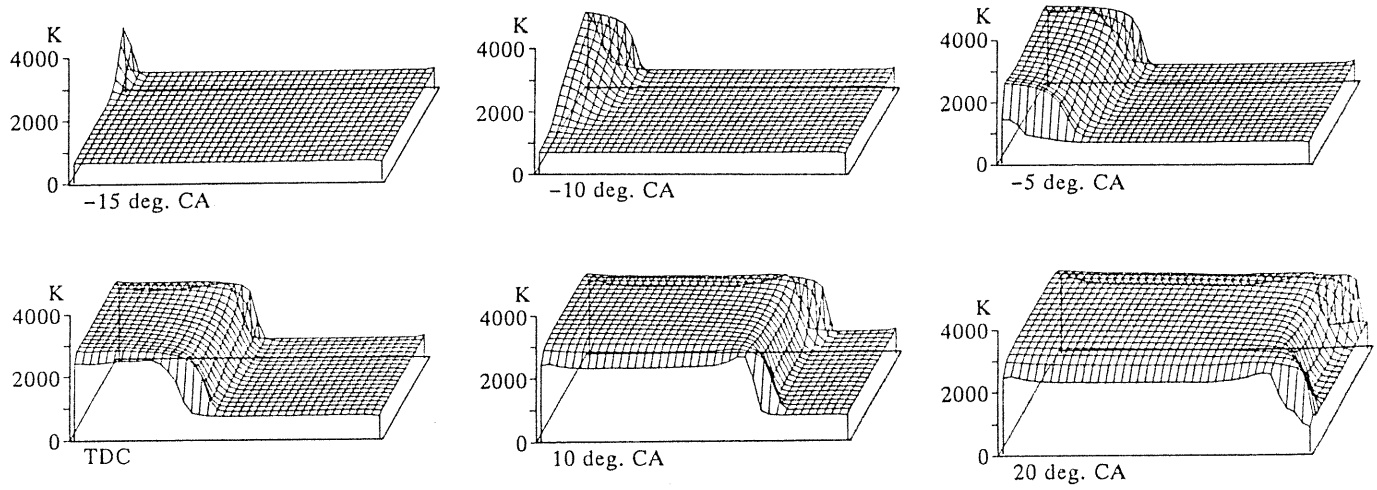

Fig. 4 Temperature fields computed for wall temperature T_w=523 K

reach the piston surface at -5 °CA. It is seen that the flame propagates towards the liner almost parallel to the piston and cylinder head surfaces from TDC through 20 °CA. The flame is seen to propagate in a nearly flat shape in the core region and to go a little ahead in the near wall regions.

The heat release rate and bulk gas temperature are shown in Fig. 5 for the three different wall temperatures as a function of crank angle. In spite of a difference between the bulk gas temperatures, the heat release rates are seen to be almost the same until around -5 °CA or the flame reaches the piston surface. This indicates that the turbulence-controlled combustion is reproduced by the present combustion model in the core region though it has the reaction term. After around -5 °CA, the combustion proceeds a little faster with increasing wall temperature. This tendency is explained from the computed result that the combustion develops faster in the near wall region due to the reaction term as the wall temperature increases.

Figure 6 shows local heat fluxes computed for the three different wall temperatures at different locations which are indicated with symbols A, B, C and D in Fig. 2. Before the flame arrival, the local heat flux at every location is seen to be lower for the elevated wall temperatures than for the conventional wall temperature, as expected from the well-known characteristics of no-reacting thermal boundary layers. It is noted that, after the flame arrival, the local heat flux rises at a faster rate, reaches higher at its peak and then descends faster than that for the conventional wall temperature as the wall temperature is elevated.

The wall temperature dependence of the local heat flux shown above was indicated in the experimental studies by Enomoto and Furuhama[3], and Takase et al.[4] who measured local heat fluxes with conventional and insulated s. i. engines.

The explanation for this characteristic is easily given by checking local heat release rates in the near wall region for the different wall temperatures as described in the following. Figure 7 shows the local heat release rate profiles at location A at different crank angles, obtained for T_w=523 K. The flame front is seen to proceed until -2 °CA and then to decay or to be quenched. The quench distance is observed between 7 μm and 15 μm. In Fig. 8, the local

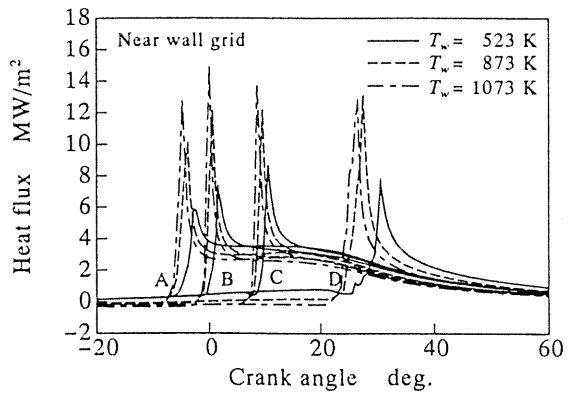

Fig. 6 Local heat fluxes for different wall temperatures

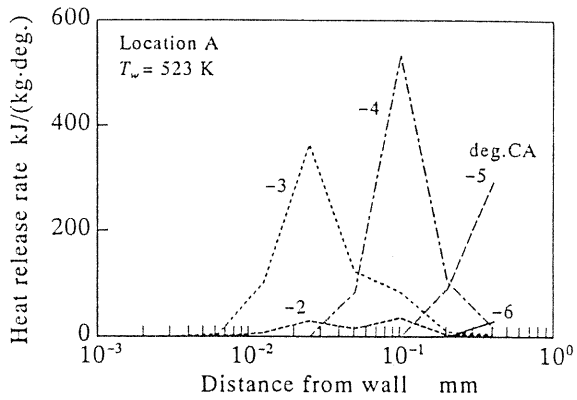

Fig. 7 Local heat release rate profiles at different times in the near wall region of location A for T_w=523 K

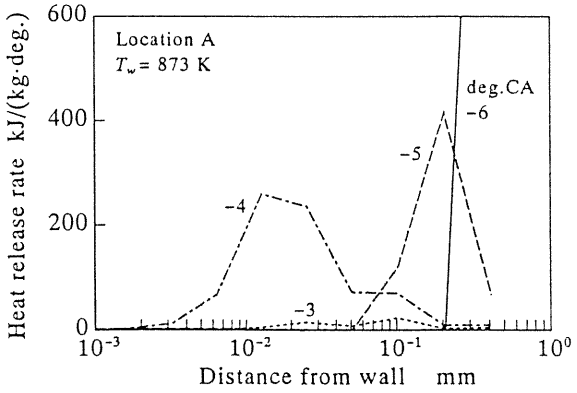

Fig. 8 Local heat release rate profiles at different times in the near wall region of location A for T_w=873 K

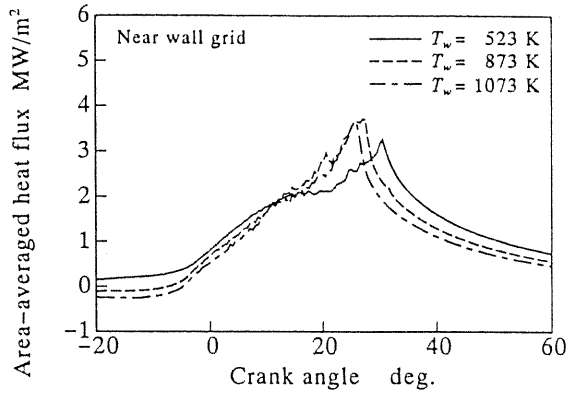

Fig. 9 Area-averaged heat fluxes for different wall temperatures

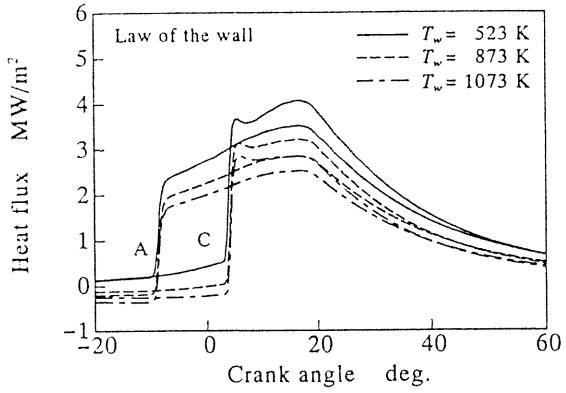

Fig. 10 Local heat fluxes for different wall temperatures computed by using the law of the wall

heat release rate profiles are shown for T_w=873 K. It is indicated that the flame develops until -4 °CA in the leading edge and the quenching takes place between 3 μm and 6 μm. It is also observable that the local heat release rate is much higher in value than that for the conventional wall temperature. The shorter quench distance and the higher local heat release rate with the elevated wall temperature can explain the augmented local heat fluxes in the peak value.

The area-averaged heat fluxes into the entire combustion chamber surface are shown in Fig. 9 for the three different wall temperatures. It is interesting to see that during the first half of the combustion period the area-averaged heat fluxes for the two elevated wall temperatures are lower than that for the conventional wall temperature, and that the tendency is reversed during the last half. The reacting thermal boundary layer exerts its effect on the wall surface so locally and short that during first half period it is not enough to overwhelm the total heat flux through the no-reacting thermal boundary layer, because the surface area exposed to the reacting thermal boundary layer is not yet so large. In the last half period, such surface area becomes larger as the flame front proceeds outward in the radial direction, making the effect of the reacting thermal boundary layer more heavily weighted.

Figure 10 shows the local heat fluxes computed by the use of the law of the wall with the same combustion model but without the near wall grid system. It is clearly seen that each local heat flux is always lower for the elevated wall temperature cases than that for the conventional wall temperature case. It can be said that the use of the law of the wall as the wall boundary condition in the CFD codes does not reproduce the experimental evidence.

CONCLUSIONS

The numerical model has been presented to analyze the unsteady thermal boundary layers with exothermic reaction in s. i. engine combustion chambers. The model features the two-stage combustion model which describes the near wall combustion as well as the core region combustion, and the near wall grid system having boundary layer resolution.

The present model reproduces the experimental evidence presented in the literatures that local heat fluxes peak higher as wall temperature is elevated, while the law of the wall does not.

The discussions on the local heat fluxes and the area-averaged heat flux indicates that exothermic reaction in thermal boundary layers plays an important role in predicting heat flux.

REFERENCES

1. Yang, J. and Martin, J. K.,"Prediction of the Effects of High Temperature Walls, Combustion, and Knock on Heat Transfer in Engine-Type Flows," SAE Paper No. 900690, 1990.
2. Jennings, M. J.,"Multi-Dimensional Modeling of Turbulent Premixed Charge Combustion," SAE Paper No.920589, 1992.
3. Enomoto, Y. and Furuhama, S.,"Heat Transfer into Ceramic Combustion Chamber Wall of Internal Combustion Engines," SAE Paper No.861276,1986.
4. Takase, S., Hosonuma, S., Yoshimura, K., Enomoto, Y., Fujiwara, Y., Fukutani, I. and Iida, N.,"Combustion and Emission of Low Heat Rejection, Ceramics Methanol ATAC Engine," Preprint, the 11th I.C.Engines Symposium, JSME/JSAE, July 14-16,1993, Tokyo, pp.399-404.
5. Morel, T. and Mansour, N. N.,"Modeling of Turbulence in Internal Combustion Engines," SAE Paper No. 820040, 1982.
6. Grimsmo, B. and Magnussen, B.F.,"Numerical Calculation of Turbulent Flow and Combustion in an Otto Engine Using the Eddy Dissipation Concept," Proc. COMODIA 90, pp. 65-73, 1990.
7. Magnussen, B.F., "The Eddy Dissipation Concept," Proc. the 15th Task Leaders Meeting/IEA, pp.177-197, 1989.
8. Westbrook, C. K. and Dryer, F. L.,"Simplified Reaction Mechanisms for the Oxidation of Hydrocarbon Fuels in Flames," Combust. Sci. Technol., Vol. 27, pp.31-43, 1981.
9. Yang, J. and Martin, J. K.,"Approximate Solution- One-Dimensional Energy Equation for Transient, Compressible, Low Mach Number Turbulent Boundary Layer Flows," J. Heat Transfer, ASME, Vol. 111, pp. 619-624, 1989.
10. Dao, K., Uyehara, O.A. and Myers, P. S.,"Heat Transfer Rate at Gas-Wall Interfaces in Motored Piston Engine," SAE Paper No. 730632, 1973.